Title	Spectroscopy of strongly deformed ^{32}Ne by proton knockout reactions
Author(s)	Murray I., MacCormick M., Bazin D., Doornenbal P., Aoi Nori, Baba Hidetada, Crawford H. L., Fallon P., Li K., Lee J., Matsushita Masafumi, Motobayashi Toru, Otsuka Takaharu, Sakurai Hiroyoshi, Scheit H., Steppenbeck D., Takeuchi Satoshi, Tostevin J. A., Tsunoda Naofumi, Utsuno Yutaka, Wang H., Yoneda Kenichiro
Citation	Physical Review C,99(1),p.011302_1-011302_7
Text Version	Published Journal Article
URL	https://jopss.jaea.go.jp/search/servlet/search?5064586
DOI	https://doi.org/10.1103/PhysRevC.99.011302
Right	

Rapid Communications

Spectroscopy of strongly deformed ^{32}Ne by proton knockout reactions

I. Murray,[1] M. MacCormick,[1] D. Bazin,[2] P. Doornenbal,[3] N. Aoi,[4] H. Baba,[3] H. Crawford,[5] P. Fallon,[5] K. Li,[3] J. Lee,[6] M. Matsushita,[3] T. Motobayashi,[3] T. Otsuka,[7,3,2,8] H. Sakurai,[3,9] H. Scheit,[10,3] D. Steppenbeck,[3] S. Takeuchi,[3] J. A. Tostevin,[11] N. Tsunoda,[7] Y. Utsuno,[12] H. Wang,[3] and K. Yoneda[3]

[1]*Institut de Physique Nucléaire, IN2P3-CNRS, Université Paris-Sud, Université Paris-Saclay, Orsay Cedex 91406, France*
[2]*National Superconducting Cyclotron Laboratory, Michigan State University, East Lansing, Michigan 48824, USA*
[3]*RIKEN Nishina Center, Wako, Saitama 351-0198, Japan*
[4]*Research Center for Nuclear Physics (RCNP), Osaka University, Ibaraki, Osaka 567-0047, Japan*
[5]*Nuclear Science Division, Lawrence Berkeley National Laboratory, Berkeley, California 94720, USA*
[6]*Department of Physics, The University of Hong Kong, Hong Kong, China*
[7]*Center for Nuclear Study (CNS), University of Tokyo, Wako-shi, Saitama 351-0198, Japan*
[8]*Instituut voor Kern-en Stralingsfysica, Katholieke Universiteit Leuven, Leuven B-3001, Belgium*
[9]*Department of Physics, University of Tokyo, 7-3-1 Hongo, Bunkyo, Tokyo 113-0033, Japan*
[10]*Technische Universität Darmstadt, 64289 Darmstadt, Germany*
[11]*Department of Physics, University of Surrey, Guildford, Surrey GU2 7XH, United Kingdom*
[12]*Japan Atomic Energy Agency, Tokai, Ibaraki 319-1195, Japan*

(Received 14 October 2018; published 7 January 2019; corrected 29 May 2019)

Low-lying states of neutron-rich ^{32}Ne were populated by means of one- and two-proton knockout reactions at the RIKEN Radioactive Isotope Beam Factory. A new transition is observed at 1410(15) keV and assigned to the $4_1^+ \rightarrow 2_1^+$ decay. With this energy the $R_{4/2}$ ratio is calculated to be 2.99(6), lying close to the rigid rotor limit and suggests a high degree of collectivity and strongest deformation among neutron-rich neon isotopes. Comparisons of experimental inclusive and exclusive reaction cross sections with shell-model and eikonal reaction dynamical calculations reveals considerable quenching for this highly asymmetric system and contributes to systematic trends.

DOI: 10.1103/PhysRevC.99.011302

Canonical magic numbers [1,2], found near the β-stability line on the Segrè chart, have wide applicability to the understanding of many facets of nuclear properties. Their existence is a consequence of nuclear shell structure and large energy gaps between groups of orbitals. In nuclear systems with unbalanced neutron and proton numbers, these magic numbers can disappear ($N = 8,\ 20,\ 28, \ldots$), and new ones precipitate in neutron-rich nuclei ($N = 16,\ 32,\ 34, \ldots$) [3]. Atomic mass trends [4] and 2_1^+ excitation energies [5–8] have provided the first clues to this phenomenon and contribute to improving our understanding of shell structure.

The first signature of the breakdown of the $N = 20$ major shell effect was the observation of excessive binding energy for sodium isotopes with ^{31,32}Na more bound than predicted [9]. This was later extended to ^{31,32}Mg [10]. A low-lying first excited 2^+ state [11,12] and the Coulomb excitation of ^{32}Mg [13,14] provided additional evidence.

This dramatic and sudden change in structure for $Z \leqslant 12$ and $N \geqslant 20$ was termed the *island of inversion* (IOI) [15] and interpreted as introduction of intruder configurations, neutron multiparticle-multihole excitations, in the ground state. The neutrons are promoted across the $N = 20$ gap from sd to pf orbitals [16] as a consequence of an increase in correlations and reduction of the spherical shell gap.

As protons are removed from the $\pi d_{5/2}$ orbital, the neutron $\nu d_{3/2}$ orbital is less bound and approaches the $\nu f_{7/2}$ and $\nu p_{3/2}$ levels, quenching the spherical $N = 20$ shell gap. The driving force of the evolution of orbitals is understood as being due to the spin-isospin components of the monopole interaction [17], the tensor force. This component of the nucleon-nucleon interaction is highlighted in increasing proton-neutron asymmetric isotopes [18].

Originally, the IOI was predicted to exist between $10 \leqslant Z \leqslant 12$ and $20 \leqslant N \leqslant 22$ [15]. However, through great experimental effort, the transition to the IOI has been revealed to be soft. Nevertheless, the borders of the IOI are not entirely delineated on the exotic south-east side, driving theoretical and experimental progress. With many studies focused on magnesium and sodium isotopes, the latter known up to $N = 24$ [19], the IOI has been barely mapped for Ne ($Z = 10$) isotopes.

For odd Ne isotopes, the ground-state spin parity reveals a soft transition from ^{27}Ne to a westward boundary of the IOI for ^{29}Ne and full inclusion into the IOI for ^{31}Ne.

Intruder configurations were suggested for ^{27}Ne through the observation of a low-lying negative-parity state $3/2^-$ [20,21]. The ground state of ^{29}Ne was established through the neutron removal cross section and a narrow parallel momentum distribution [22], thus supporting the

ground state as largely consisting of a $^{28}\mathrm{Ne}(0_1^+) \otimes 2p_{3/2}$ neutron intruder configuration. ^{31}Ne is suggested to exhibit a p-wave halo structure of ground-state spin-parity $3/2^-$ by observation of a large Coulomb breakup cross section [23] and one-nucleon removal reactions [24].

For even Ne isotopes a soft transition is also reported from ^{28}Ne and admittance of ^{30}Ne and ^{32}Ne within the IOI. ^{28}Ne is observed to have a significantly lowered 2_1^+ energy level ($E2_1^+$) [14], a characteristic signature of increasing collectivity. The low excited first 2_1^+ state and reduced $E2$ transition probability of ^{30}Ne indicates a large enhancement in collectivity and firmly places it within the IOI [25,26]. The first excited 2_1^+ state at 722(9) keV [27] by in-beam spectroscopy of the near drip-line nucleus ^{32}Ne ($N = 22$) has been identified. The low-level energy and predictions by shell-model calculations [28,29] reveal a continuing trend of strong deformation and a ground state dominated by intruder configurations [27]. ^{32}Ne is the most neutron-rich neon isotope known to belong to the IOI, and understanding the role of intruder configurations to the yet unknown drip line commands further study.

Here, we present an in-beam spectroscopic study of ^{32}Ne to extend its limited level scheme and to determine inclusive and exclusive cross sections by one- and two-proton knockout reactions. These reactions directly probe the active orbitals near the Fermi surface via the one- and two-particle overlaps of the wave functions of the projectiles (^{33}Na and ^{34}Mg) and the final states of the reaction product (^{32}Ne). They also add information on the nucleon removal cross section trends for highly asymmetric systems.

For one-nucleon removal experiments, the growing data set for the ratio of the measured inclusive cross section to the calculated one ($R_s = \sigma_{\mathrm{ex}}/\sigma_{\mathrm{th}}$), shows greater suppression when removing a nucleon from the minority species in more asymmetric systems [30,31]. In two-nucleon (2N) removal reactions the requirement that the reaction is direct [32,33] and not contaminated by sequential processes has restricted the analogous comparisons to involve well-bound minority species as for the ^{9}Be(^{34}Mg, ^{32}Ne)X reaction here. No asymmetry dependence in the 2N removal cross section ratio R_s has been established. This ratio has been shown to be close to 0.5 for several sd-shell systems [34] but with greater suppression observed when there are large structural and/or deformation changes between the initial and the final states [35,36], situations which challenge truncated basis shell-model calculations.

The present experiment was performed at the BigRIPS fragment separator and ZeroDegree spectrometer [37] at the Radioactive Isotope Beam Factory (RIBF), operated by the RIKEN Nishina Center and the Center for Nuclear Study, University of Tokyo. Secondary radioactive cocktail beams of ^{33}Na (2%) and ^{34}Mg (21%) were produced by projectile fragmentation of a 345 MeV/u primary beam of ^{48}Ca on a 15-mm-thick rotating Be target. The average beam intensity was 90 pnA. Secondary beams were purified via the $B\rho - \Delta E - B\rho$ method using dipoles and 5-mm-thick aluminum degraders on dispersive focal planes. Event-by-event identification of the secondary beam particles in BigRIPS

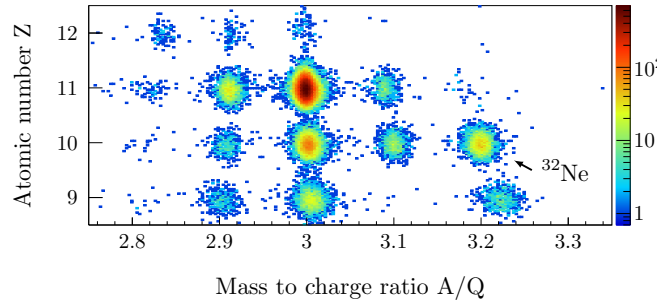

FIG. 1. The ZeroDegree spectrometer particle identification of predominantly fully stripped reaction residues after the ^{9}Be secondary reaction target.

was accomplished by the TOF $- B\rho - \Delta E$ method, wherein the time of flight (TOF), magnetic rigidity, and energy loss were used to determine the mass-to-charge ratios (A/Q) and atomic numbers (Z) [38]. The rates of secondary beams of ^{33}Na and ^{34}Mg were 85 and 8000 particles per second, respectively.

A 1032-mg/cm^2-thick Be solid target located at focal plane $F8$-induced secondary reactions and the products of which were transmitted to the ZeroDegree spectrometer. The magnetic rigidity of BigRIPS and ZeroDegree spectrometers were set to maximize transmission of ^{34}Mg projectiles and two-proton knockout reaction residues ^{32}Ne. The large momentum acceptance of the ZeroDegree spectrometer (8%) permitted simultaneous acceptance of one-proton knockout residues from ^{33}Na. The midtarget beam energies were 235 and 221 MeV/u for ^{34}Mg and ^{33}Na, respectively.

The TOF $- B\rho - \Delta E$ method was likewise implemented for the identification of reaction residues in the ZeroDegree spectrometer. A particle identification diagram is presented in Fig. 1 and shows a clear separation of ^{32}Ne.

To observe the decay of short-lived populated states the DALI2 γ spectrometer [39], composed of 186 NaI(Tl) crystals, encompassed the secondary target with an angular coverage of 18–148°. Calibrations were completed using ^{88}Y, ^{60}Co, and ^{137}Cs sources. In the γ-ray reconstruction, an energy add-back procedure was applied within a radius of 15 cm between hit detectors to increase photopeak efficiency and a multiplicity threshold of 3 was selected. A GEANT4-based [40] simulation of the DALI2 array was utilized to produce full response functions based on individual detector energy resolutions and thresholds, mean beam velocity, energy loss in the target [41], and state lifetime.

The Doppler-reconstructed spectra of both one- and two-proton knockout reactions to ^{32}Ne are presented in Fig. 2. A strong transition at 709(12) keV, combining observations in both reactions, corresponds to the $2_1^+ \rightarrow 0_{\mathrm{g.s.}}^+$ transition and is consistent with a previous measurement of 722(9) keV by both inelastic scattering and proton removal with lower statistics [27]. A new transition at 1410(15) keV was observed from the one- and two-proton knockout reactions. The background-subtracted $\gamma\gamma$ coincidence spectrum of Fig. 2(b), obtained with the condition of a prompt coincidence with this new transition, indicates a decay sequence with the 722(9)-keV transition with a relative intensity of 108(20)%.

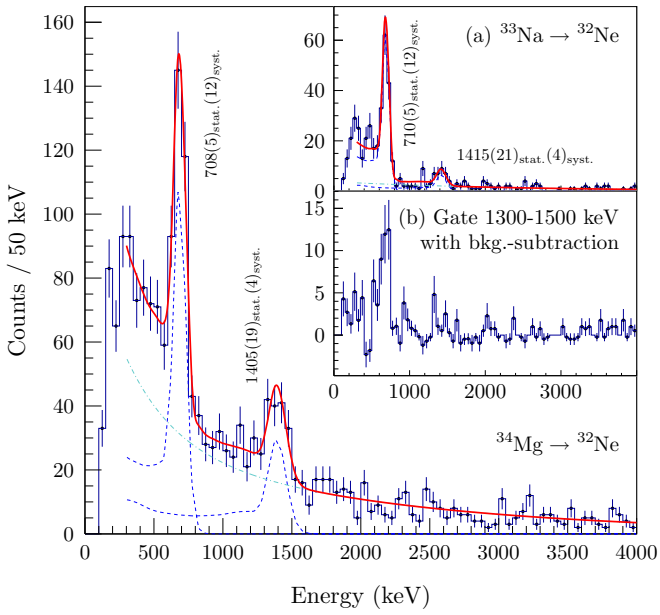

FIG. 2. Doppler-reconstructed γ-ray energy spectrum of two-proton and (a) one-proton knockout reactions leading to ^{32}Ne. A least-squares fit (red solid line) of a global function composed of simulated responses of DALI2 (dotted blue) and a two-component exponential background (dotted cyan) is applied. (b) Background-subtracted $\gamma\gamma$ coincidence spectrum of combined one- and two-proton knockout reactions for a 1410-keV transition (1300–1500-keV gate and 1600–3000-keV background region).

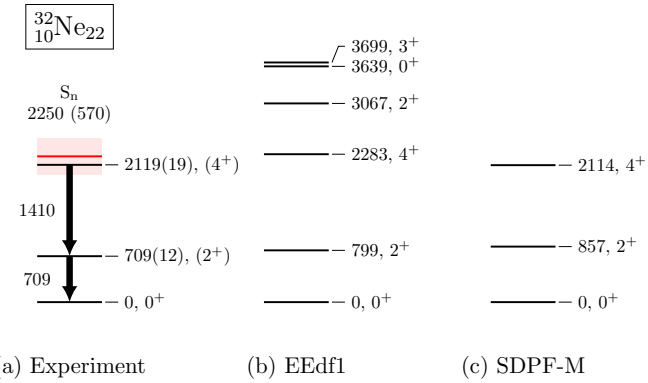

FIG. 3. (a) Energy levels from the present experiment compared to (b) EEdf1 [42] and (c) SDPF-M [28] effective interaction shell-model calculations for ^{32}Ne. The extrapolated neutron separation energy (S_n) of 2250(570) keV [43] is shown in red. The uncertainty is shown as the width.

The 1410(15)-keV transition is tentatively assigned to the $4_1^+ \rightarrow 2_1^+$ decay. Spin and parity assignment is based on: (i) prompt coincidence with the $2_1^+ \rightarrow 0^+_{g.s.}$ transition, (ii) population of 4_1^+ states in proton knockout reactions to ^{28,30}Ne with fast beams [32,35], (iii) the reproduction of energy levels with shell-model calculations, (iv) reaction theory exclusive cross section ratios as will be discussed later in the text, and (v) the limited possibility of additional bound states due to a low extrapolated neutron separation energy (S_n) of 2250(570) keV [43].

A global parametric function, composed of a DALI2 response function and a two-component exponential background, fit to the reconstructed experimental spectra was used to extract the energies and intensities of the transitions. Doppler reconstructions were performed at the target center. The uncertainty in the deduced transition energies include a statistical contribution, detector calibration errors, uncertainty in beam energy, and uncertainty from the unmeasured lifetime of the 2_1^+ state. The lifetime of the 2_1^+ state was chosen to be 60 ps as predicted by global trends [44]. Variation of this lifetime by a factor of 2 produces a shift of the $2_1^+ \rightarrow 0^+_{g.s.}$ transition by 10 keV and is the largest contribution to the systematic uncertainty. The 2_1^+ lifetime is a small uncertainty component (1 keV) in the $4_1^+ \rightarrow 2_1^+$ transition uncertainty.

In addition to the experimentally determined states, shell-model calculations with large valence spaces have been performed. The recently available extended Kuo-Krenciglowa (EKK) derived effective interaction [42], henceforth called EEdf1, includes multiparticle-multihole transition mixing across the $N = 20$ shell gap in a complete $sdpf$ model space. This is compared to the SDPF-M interaction [28], restricted to the sd-$p_{3/2}f_{7/2}$ space but which allows for mixing of sd and pf configurations. Both interactions have been shown to provide a good description of the IOI and predict strongly deformed ground states dominated by intruder configurations for $N = 20$ neon and magnesium isotopes.

The predicted states are in agreement with the experimentally assigned levels in ^{32}Ne as shown in Fig. 3. The lowered 2_1^+ and 4_1^+ states are reproduced with both shell-model calculations anticipating a less developed rotational band. The observed states and ground state are found to be almost pure intruder configurations with the EEdf1 interaction. They are composed mainly of 2p-2h ($\approx$40%) and 4p-4h ($\approx$50%) components as presented in Table I. In addition, the $R_{4/2}$ ratio, defined as the ratio of $E4_1^+$ and $E2_1^+$ energies, is predicted to increase to a maximum at $N = 22$. Confirmation of this increase is established from the newly deduced 4_1^+ state energy and is thus the highest experimental $R_{4/2}$ ratio in the neutron-rich neon isotopic chain. These observations provide additional experimental evidence for the inclusion of ^{32}Ne inside the *island of inversion*.

The experimental and predicted 2_1^+ and 4_1^+ energy levels and $R_{4/2}$ ratios of neutron-rich silicon, magnesium, and neon isotopes are shown in Fig. 4 and display signatures of shell evolution. The peak in $E2_1^+$ for silicon at $N = 20$ is an

TABLE I. ^{32,34}Mg and ^{30,32}Ne ground-state neutron 0p-0h, 2p-2h, and 4p-4h probabilities (%) calculated with the SDPF-M and EEDf1 interactions.

	SDPF-M			EEDf1		
	0p-0h	2p-2h	4p-4h	0p-0h	2p-2h	4p-4h
^{32}Mg	4.7	82.5	12.7	1.8	36.2	51.9
^{30}Ne	3.9	74.1	22.0	0.5	19.8	68.1
^{34}Mg	9.5	82.0	8.4	1.6	49.5	43.4
^{32}Ne	10.0	76.5	13.4	1.2	43.3	50.6

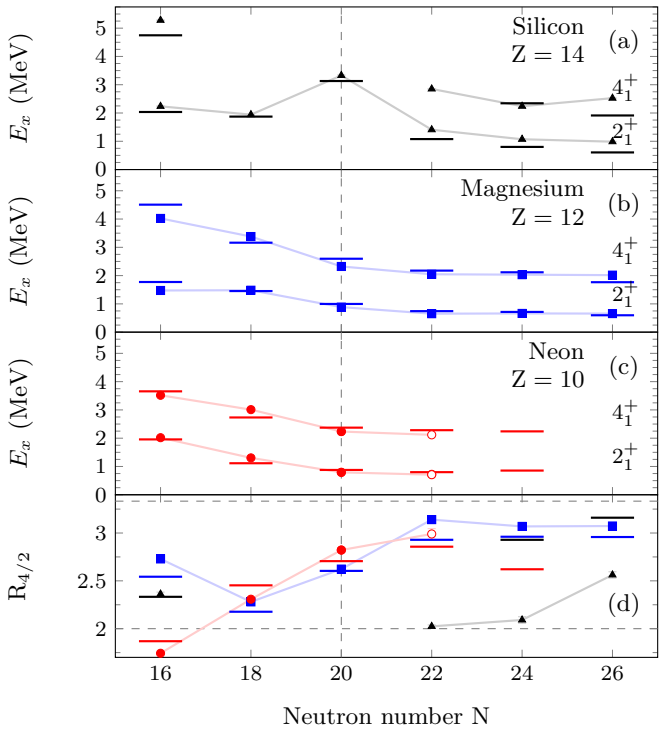

FIG. 4. Systematics of experimental first excited 2_1^+ and 4_1^+ levels across $16 \leqslant N \leqslant 26$ for (a) silicon (black, triangle), (b) magnesium (blue, square), and (c) neon (red, circle). Open circles are measured in this Rapid Communication. Connecting lines are drawn to guide the eye. Horizontal bars are calculations with EEdf1 effective interaction [42]. (d) $R_{4/2}$ values. Dashed horizontal lines for vibrational (2.0) and rotational limits (3.33) are drawn. Experimental data were taken from Refs. [45–51].

indication of a good shell closure, in contrast to the low $E2_1^+$ and $E4_1^+$ for magnesium and neon. Furthermore, the increasing $R_{4/2}$ ratio is emblematic of a developing quadrupole collectivity in magnesium, and this new measurement confirms the continuation of a similar trend in neon for $N > 20$.

Direct reaction theory is combined with the shell-model overlaps, given by the spectroscopic factors (C^2S) and two-nucleon amplitudes (TNAs), respectively, to calculate the exclusive and inclusive one- and two-proton removal cross sections to ^{32}Ne. The sudden (fast collisions) and eikonal (forward-scattering) approximations are applied [33,34,52,53]. Details of the inputs to the reaction calculations and of the use of Hartee-Fock calculations to constrain the projectile-target distorting interactions and the proton bound-state potential geometries are discussed in Refs. [30,31] and [33,34]. The direct nature of the two-proton removal mechanism is guaranteed by the energetics involved in the removal of the well-bound protons [32,33]. The asymmetry in the ^{33}Na separation energies for protons [20.510(680) MeV] and neutrons [2.930(450) MeV] suppresses the competing proton evaporation channel following the population of highly excited ^{33}Na nuclei via one-proton removals from ^{34}Mg.

The ^{9}Be target induces reactions proceeding by elastic (diffraction dissociation) and inelastic (stripping) processes. These mechanisms are calculated separately by reaction theory and are indistinguishable in this experiment. Their relative contributions have been studied previously [54,55] and were shown to be in good agreement with eikonal model predictions for reactions involving both strongly and weakly bound nucleons. Given the strong binding of the protons in the present cases, the stripping mechanism is dominant.

The experimental cross sections were determined by the number of projectiles and fragments in BigRIPS and ZeroDegree spectrometers, respectively. Corrections for tracking efficiency, indistinguishable reactions in the 1-mm plastic scintillator before the target, and acquisition dead time were applied. Uncertainties in the target areal density, transmission, and reaction contaminants are included.

The calculated inclusive two-proton removal reaction cross section (to the two shell-model states below the neutron separation threshold) is 530 μb based on the TNA of the EEdf1 shell-model interaction. This is significantly greater than the measured inclusive cross section of 144(15) μb. The accompanying inclusive suppression factor $R_s(2N)$ is 0.27(3) with the EEdf1 interaction shell-model TNAs. Detailed results are presented in Table II.

The suppression factor $R_s(2N)$ is consistent with the trend from previous experiments and analysis for neon isotopes as shown in Fig. 5(b) and may signal a saturation of $R_s(2N)$

TABLE II. One- and two-proton knockout cross sections (σ) for ^{9}Be(^{33}Na, ^{32}Ne)X and ^{9}Be(^{34}Mg, ^{32}Ne)X reactions. Spin and parity assignment J^π, excitation energy E_x, transition energy E_γ, calculated single-particle cross section σ_{sp}, shell-model spectroscopic factor C^2S for the one-proton knockout reaction, and theoretical and experimental individual cross section σ^{th} and σ^{exp}, respectively. The inclusive suppression factors are 0.37(4) for the ^{9}Be(^{33}Na, ^{32}Ne)X reaction ($\Delta S = +18.37$) and 0.27(3) for the ^{9}Be(^{34}Mg, ^{32}Ne)X reaction calculated with the EKK-SDPF interaction.

						^{9}Be(^{33}Na, ^{32}Ne)X EEdf1			^{9}Be(^{34}Mg, ^{32}Ne)X EEdf1	^{9}Be(^{34}Mg, ^{32}Ne)X SDPF-M	
J^π	E_x (keV)	E_γ (keV)	$n\ell_j$	C^2S	σ_{sp} (mb)	σ^{th}_{-1p} (mb)	σ^{th}_{-1p} (mb)	σ^{exp}_{-1p} (mb)	σ^{th}_{-2p} (μb)	σ^{th}_{-2p} (μb)	σ^{exp}_{-2p} (μb)
0			$0d_{3/2}$	0.026	9.53	0.262	0.262	1.4(7)	355	387	97(14)
2	709(12)	709(12)	$1s_{1/2}$	0.010	9.91	0.101	9.563	2.2(6)	17	34.8	24(9)
			$0d_{3/2}$	0.037	9.37	0.367					
			$0d_{5/2}$	0.864	9.89	9.095					
4	2119(19)	1410(15)	$0d_{5/2}$	0.169	9.58	1.721	1.721	0.72(3)	158	241	23(5)
			Inclusive:				11.55	4.3(5)	530	664	144(15)

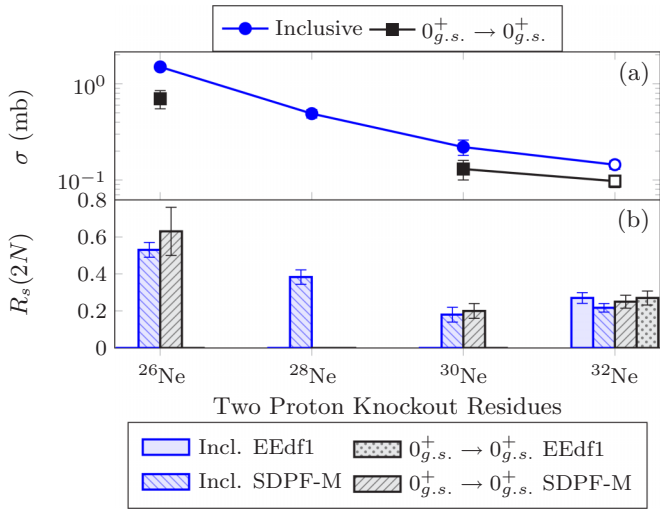

FIG. 5. (a) Two-proton knockout experimental inclusive and $0^+_{\text{g.s.}} \rightarrow 0^+_{\text{g.s.}}$ cross sections (σ). Data taken from Refs. [32,34,35]. (b) $R_s(2N)$ suppression factors utilizing EEdf1 and SDPF-M interactions. The theoretical inclusive cross sections to ^{26}Ne and ^{28}Ne are calculated with the eikonal reaction framework, described in this Rapid Communication, to be 2.82 and 1.28 mb. The associated inclusive $R_s(2N)$'s for ^{26}Ne and ^{28}Ne are 0.53(4) and 0.38(4).

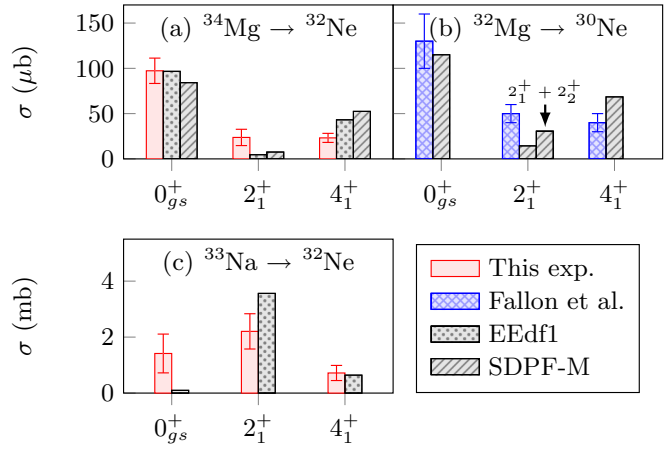

FIG. 6. Experimental exclusive cross sections and theoretical predictions from shell-model calculations. Exclusive theoretical cross sections are scaled by the inclusive R_s value for the visualization of the populated ratio. (a) Two-proton knockout reactions to $^{32}_{10}$Ne [35]. The theoretical cross section to the 2^+_1 state was conjectured to include unobserved feeding from a 2^+_2 state. This combined cross section is also plotted. (c) One-proton knockout reactions to $^{32}_{10}$Ne.

values. In the case of the two-proton removal reaction to ^{30}Ne [35], the small $R_s(2N)$ value was interpreted as due to a change in neutron configuration between ^{32}Ne and ^{30}Ne ground states, absent from the SDPF-M interaction shell-model calculations. Assuming a dominant 2p-2h neutron configuration in ^{32}Mg, consistent with SDPF-M, this interpretation implied a significant ($\approx$50%) 4p-4h component in ^{30}Ne. Shell-model calculations with the EEdf1 interaction predict higher 4p-4h components in both ^{30}Ne and ^{32}Mg as well as ^{32}Ne and ^{34}Mg ground states as shown in Table I. However, the TNA from the two interactions are not drastically different, and this is reflected by the similar calculated suppression factors $R_s(2N)$ shown in Fig. 5(b). As a result, it is not possible to firmly establish the $R_s(2N)$ value as a missing structural difference present in the TNAs or a consequence of the reaction theory framework. No general trend of $R_s(2N)$ has been established, unlike for one-nucleon knockout reactions.

In the case of the one-proton knockout reaction ^{9}Be(^{33}Na, ^{32}Ne)X, the calculated inclusive cross section, based on the EEdf1 interaction shell-model spectroscopic factors, is 11 mb. The experimental inclusive cross section is 4.3(5) mb. Thus, the suppression factor is 0.37(4) and the associated separation-energy asymmetry $\Delta S = S_p - S_n = +18.37$ MeV. This value falls entirely within and adds to the one-nucleon removal trend shown in Fig. 1 of Ref. [30]. Short and collective long-range correlations unaccounted for in shell-model calculations have been suggested to contribute to the one-nucleon suppression factor for stable nuclei [56]. Measurements of electron-induced proton knockout reactions for nuclei close to stability have revealed quenching of the spectroscopic strengths on the order of $\approx$30% [56,57]. Given the intertwined nature of shell-model C^2S and reaction formalism (and inputs) to calculate a theoretical cross section, it is not possible to identify a direct contributor to the one-nucleon cross section deviation. However, recent transfer reaction experiments as a spectroscopic probe, display a weak dependence of the reduction factors and correlations as a function of Fermi-surface asymmetry [58–60].

The determination of experimental exclusive cross sections for both one- and two-proton knockout reactions requires the observation of transitions with the DALI2 spectrometer and a fit to the GEANT4-simulated response functions. A 6% uncertainty was included to account for a difference between the simulated and measured DALI2 efficiency. The following assumptions were made in the determination of the direct population of states in ^{32}Ne: (i) 4^+ feeds directly to the 2^+ state in a cascade, (ii) and no feeding from higher unobserved states is present. To compare the ratio to each state to theoretical predictions, the theoretical cross sections are scaled by the inclusive suppression factor and are shown in Fig. 6.

The trend of populating the excited states is reproduced by the theoretical calculations for both one- and two-proton knockout reactions. These support the spin assignments made to the two observed transitions in ^{32}Ne. The $2p$-knockout reaction follows a similar sequence as the $2p$-knockout reaction to ^{30}Ne [35] with both displaying similar 4^+ and 2^+ fractions, whereas the largest strength feeds directly to the ground state. For the case of the $1p$ knockout, the small theoretical cross section to $0^+_{\text{g.s.}}$ reflects the small occupancy of the proton $0d_{3/2}$ orbital in the ^{33}Na ground state.

To summarize, a new transition of 1410(15) keV was identified in one- and two-proton knockout reactions to ^{32}Ne at 221 and 235 MeV/u using the DALI2 γ spectrometer and BigRIPS and ZeroDegree spectrometers. This transition was assigned to the $4^+_1 \rightarrow 2^+_1$ transition based on systematics, excellent agreement with shell-model calculations and reaction

theory, and the limited expectation of additional bound states. This first $R_{4/2}$ ratio of 2.99(6) indicates a continuation of the trend of increasing collectivity above $N > 20$ for neon as well as further evidence for the incorporation of this nuclide within the *island of inversion*. A measurement of inclusive and exclusive cross sections in the two-proton knockout reaction revealed a significant suppression factor R_s as seen with ^{30}Ne [35]. A similarly reduced suppression factor was measured for the one-proton knockout reaction. Extending spectroscopic investigations to the potential drip-line nucleus ^{34}Ne [61,62], to confirm the merging of the $N = 20$ and $N = 28$ islands of inversion in neon [63] will be a challenge for future experimental facilities and demands further development in both RI production and γ detection sensitivity.

The authors wish to express their gratitude to the RIKEN Nishina RIBF accelerator staff and the BigRIPS team for providing the high intensity beams which made this experiment possible. I.M. acknowledges the support of the RIKEN IPA Program and enlightening discussions with F. Flavigny. J.A.T. acknowledges support from the Science and Technology Facilities Council (U.K.) Grant No. ST/L005743/1.

[1] M. G. Mayer, Phys. Rev. **74**, 235 (1948).
[2] O. Haxel, J. H. D. Jensen, and H. E. Suess, Phys. Rev. **75**, 1766 (1949).
[3] O. Sorlin and M.-G. Porquet, Prog. Part. Nucl. Phys. **61**, 602 (2008).
[4] F. Wienholtz, *et al.*, Nature (London) **498**, 346 (2013).
[5] C. Hoffman *et al.*, Phys. Lett. B **672**, 17 (2009).
[6] K. Tshoo *et al.*, Phys. Rev. Lett. **109**, 022501 (2012).
[7] D. Steppenbeck *et al.*, Nature (London) **502**, 207 (2013).
[8] B. Bastin *et al.*, Phys. Rev. Lett. **99**, 022503 (2007).
[9] C. Thibault *et al.*, Phys. Rev. C **12**, 644 (1975).
[10] D. J. Vieira, J. M. Wouters, K. Vaziri, R. H. Kraus, Jr., H. Wollnik, G. W. Butler, F. K. Wohn, and A. H. Wapstra, Phys. Rev. Lett. **57**, 3253 (1986).
[11] C. Détraz, D. Guillemaud, G. Huber, R. Klapisch, M. Langevin, F. Naulin, C. Thibault, L. C. Carraz, and F. Touchard, Phys. Rev. C **19**, 164 (1979).
[12] D. Guillemaud-Mueller *et al.*, Nucl. Phys. **A426**, 37 (1984).
[13] T. Motobayashi *et al.*, Phys. Lett. B **346**, 9 (1995).
[14] B. Pritychenko *et al.*, Phys. Lett. B **461**, 322 (1999).
[15] E. K. Warburton, J. A. Becker, and B. A. Brown, Phys. Rev. C **41**, 1147 (1990).
[16] A. Poves and J. Retamosa, Phys. Lett. B **184**, 311 (1987).
[17] T. Otsuka, R. Fujimoto, Y. Utsuno, B. A. Brown, M. Honma, and T. Mizusaki, Phys. Rev. Lett. **87**, 082502 (2001).
[18] T. Otsuka, T. Suzuki, R. Fujimoto, H. Grawe, and Y. Akaishi, Phys. Rev. Lett. **95**, 232502 (2005).
[19] P. Doornenbal *et al.*, Prog. Theor. Exp. Phys. **2014**, 053D01 (2014).
[20] A. Obertelli *et al.*, Phys. Lett. B **633**, 33 (2006).
[21] J. Terry *et al.*, Phys. Lett. B **640**, 86 (2006).
[22] N. Kobayashi *et al.*, Phys. Rev. C **93**, 014613 (2016).
[23] T. Nakamura *et al.*, Phys. Rev. Lett. **103**, 262501 (2009).
[24] T. Nakamura *et al.*, Phys. Rev. Lett. **112**, 142501 (2014).
[25] Y. Yanagisawa *et al.*, Phys. Lett. B **566**, 84 (2003).
[26] P. Doornenbal, H. Scheit, S. Takeuchi, N. Aoi, K. Li, M. Matsushita, D. Steppenbeck, H. Wang, H. Baba, E. Ideguchi, N. Kobayashi, Y. Kondo, J. Lee, S. Michimasa, T. Motobayashi, A. Poves, H. Sakurai, M. Takechi, Y. Togano, and K. Yoneda, Phys. Rev. C **93**, 044306 (2016).
[27] P. Doornenbal *et al.*, Phys. Rev. Lett. **103**, 032501 (2009).
[28] Y. Utsuno, T. Otsuka, T. Mizusaki, and M. Honma, Phys. Rev. C **60**, 054315 (1999).
[29] E. Caurier, F. Nowacki, and A. Poves, Nucl. Phys. **A693**, 374 (2001).
[30] J. A. Tostevin and A. Gade, Phys. Rev. C **90**, 057602 (2014).
[31] A. Gade *et al.*, Phys. Rev. C **77**, 044306 (2008).
[32] D. Bazin, B. A. Brown, C. M. Campbell, J. A. Church, D. C. Dinca, J. Enders, A. Gade, T. Glasmacher, P. G. Hansen, W. F. Mueller, H. Olliver, B. C. Perry, B. M. Sherrill, J. R. Terry, and J. A. Tostevin, Phys. Rev. Lett. **91**, 012501 (2003).
[33] J. A. Tostevin, G. Podolyák, B. A. Brown, and P. G. Hansen, Phys. Rev. C **70**, 064602 (2004).
[34] J. A. Tostevin and B. A. Brown, Phys. Rev. C **74**, 064604 (2006).
[35] P. Fallon *et al.*, Phys. Rev. C **81**, 041302 (2010).
[36] A. Gade *et al.*, Phys. Rev. Lett. **99**, 072502 (2007).
[37] T. Kubo *et al.*, Prog. Theor. Exp. Phys. **2012**, 3C003 (2012).
[38] N. Fukuda *et al.*, Nucl. Instrum. Methods Phys. Res., Sect. B **317**, 323 (2013).
[39] S. Takeuchi *et al.*, Nucl. Instrum. Methods Phys. Res., Sect. A **763**, 596 (2014).
[40] S. Agostinelli *et al.*, Nucl. Instrum. Methods Phys. Res., Sect. A **506**, 250 (2003).
[41] H. Geissel, C. Scheidenberger, P. Malzacher, and J. Kunzendorf, ATIMA, calculating atomic interaction with matter.
[42] N. Tsunoda, T. Otsuka, N. Shimizu, M. Hjorth-Jensen, K. Takayanagi, and T. Suzuki, Phys. Rev. C **95**, 021304(R) (2017).
[43] M. wang *et al.*, Chinese Phys. C **41**, 030003 (2017).
[44] S. Raman, C. Nestor, and P. Tikkanen, At. Data Nucl. Data Tables **78**, 1 (2001).
[45] M. Basunia and A. Hurst, Nucl. Data Sheets **134**, 1 (2016).
[46] M. S. Basunia, Nucl. Data Sheets **114**, 1189 (2013).
[47] M. S. Basunia, Nucl. Data Sheets **111**, 2331 (2010).
[48] N. Nica and B. Singh, Nucl. Data Sheets **113**, 1563 (2012).
[49] P. Doornenbal *et al.*, Phys. Rev. Lett. **111**, 212502 (2013).
[50] N. Nica, J. Cameron, and B. Singh, Nucl. Data Sheets **113**, 1 (2012).
[51] S. Takeuchi *et al.*, Phys. Rev. Lett. **109**, 182501 (2012).
[52] J. A. Tostevin, Nucl. Phys. A **682**, 320 (2001).
[53] P. Hansen and J. Tostevin, Annu. Rev. Nucl. Sci. **53**, 219 (2003).
[54] D. Bazin *et al.*, Phys. Rev. Lett. **102**, 232501 (2009).
[55] K. Wimmer, D. Bazin, A. Gade, J. A. Tostevin, T. Baugher, Z. Chajecki, D. Coupland, M. A. Famiano, T. K. Ghosh, G. F. Grinyer, M. E. Howard, M. Kilburn, W. G. Lynch, B. Manning, K. Meierbachtol, P. Quarterman, A. Ratkiewicz, A. Sanetullaev, R. H. Showalter, S. R. Stroberg, M. B. Tsang, D. Weisshaar, J. Winkelbauer, R. Winkler, and M. Youngs, Phys. Rev. C **90**, 064615 (2014).

[56] W. Dickhoff and C. Barbieri, Prog. Part. Nucl. Phys. **52**, 377 (2004).
[57] V. R. Pandharipande, I. Sick, and P. K. deWitt Huberts, Rev. Mod. Phys. **69**, 981 (1997).
[58] J. Lee *et al.*, Phys. Rev. Lett. **104**, 112701 (2010).
[59] J. Lee *et al.*, Phys. Rev. C **83**, 014606 (2011).
[60] F. Flavigny *et al.*, Phys. Rev. Lett. **110**, 122503 (2013).
[61] M. Notani *et al.*, Phys. Lett. B **542**, 49 (2002).
[62] S. Lukyanov *et al.*, J. Phys. G: Nucl. Part. Phys. **28**, L41 (2002).
[63] E. Caurier, F. Nowacki, and A. Poves, Phys. Rev. C **90**, 014302 (2014).

Correction: Abbreviations for chemical elements were presented incorrectly at several locations in text, tables, and table captions and have been fixed.